Dislocation dynamics analysis of dislocation intersections in nanoscale metallic multilayered composites

F. Akasheh[a] and H. M. Zbib
School of Mechanical and Materials Engineering, Washington State University, Pullman, Washington 99164-2920

J. P. Hirth, R. G. Hoagland, and A. Misra
MST Division, Los Alamos National Laboratory, Los Alamos, New Mexico 87545

(Received 28 August 2006; accepted 25 February 2007; published online 30 April 2007)

In this work, dislocation dynamics (DD) analysis is used to investigate the strength of nanoscale metallic multilayered composites. Several possible interactions between threading (glide) dislocations and intersecting interfacial dislocations are considered and found to lead to strength predictions in better agreement with experimental trends and significantly higher than the predictions of the simplified confined layer plasticity model based on Orowan bowing of single dislocation in a rigid channel. The strongest interaction occurs when threading and intersecting interfacial dislocations have collinear Burgers' vector and involves an annihilation reaction at their crossing points followed by the resumption of threading with a new dislocation configuration. The other possible dislocation intersections involve the formation of junctions, which are found to be more complex than simple models suggest. When the layer interfaces are modeled as impenetrable walls, as in existing analytical and some dislocation dynamics (DD) models, the predicted strengthening effect is weaker than that predicted by DD with more physical boundary conditions at the interfaces. © *2007 American Institute of Physics*. [DOI: 10.1063/1.2721093]

I. INTRODUCTION

Nanoscale metallic multilayered (NMM) composites represent an important class of advanced engineering materials due to their unusually high strength, several times larger than the rule-of-mixture prediction, and ductility among other favorable properties. Typically, NMM composites are made of bimetallic systems, built into alternating layers of equal thickness, with individual layer thickness on the order of a few to tens of nanometers, by vapor- or electrodeposition. Careful experiments by several groups have clearly demonstrated that such materials exhibit a combination of superior mechanical properties: ultrahigh strength reaching 1/3 to 1/2 of the theoretical strength of any of the constituent materials,[1–5] high ductility,[6] morphological stability under high temperatures[7] and after large deformation,[6] enhanced fatigue resistance,[8,9] and improved irradiation damage resistance.[10] In this article, we focus our attention on understanding the deformation mechanisms and their contribution to the high strength of NMM composites.

Figure 1 shows the scale dependence of yield strength of multilayered structures. In Regime I (hundreds of nanometers and above) the strength can be well described by the Hall-Petch relation with the individual layer thickness acting as the characteristic length scale. Deformation in this regime is characterized by the formation of dislocation cell structure in the interior of the layers and dislocation pileups at the interfaces. In Regime II, the nanoscale range of interest to us here, the strength continues to increase as the layer thickness decreases; however, the dependence deviates from the Hall-Petch relation. Furthermore, no cell structure formation in the layer interior is observed upon deformation. Both observations indicate a fundamental difference in the active dislocation mechanisms at the two scales. While Frank-Read source operation leading to dislocation pileups is possible in the micrometer range, it becomes increasingly difficult as the layer thickness decreases, ultimately ceasing. Instead, glide of what is known as threading dislocations is believed to be the primary plasticity mechanism at the nanoscale.[11–13] Threading dislocations originate as faults in the atom arrangement during the deposition process and, once formed in one layer, replicate themselves in the next overlaid layer and so on. They are perfect glide dislocations, inhabiting typical glide planes and having Burgers' vectors of type $a/2\langle 110\rangle$ in fcc crystals, and stretch along the glide planes between the interfaces. When the stress in the layer is high enough, a threading dislocation glides on its slip plane, depositing in its

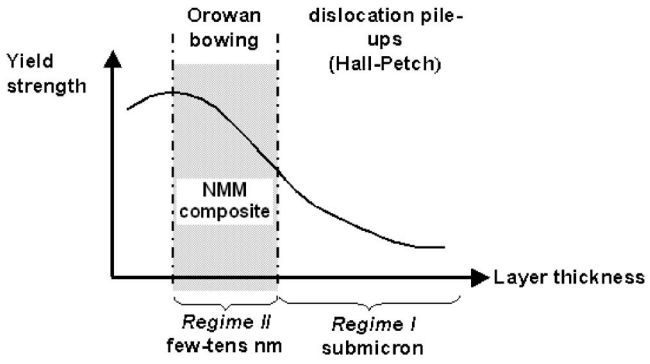

FIG. 1. Schematic showing dependence of yield strength of multilayered structures on the individual layer thickness.

[a]Electronic mail: fakasheh@mail.wsu.edu

 © 2007 American Institute of Physics

Downloaded 03 Nov 2009 to 128.12.160.33. Redistribution subject to AIP license or copyright; see http://jap.aip.org/jap/copyright.jsp

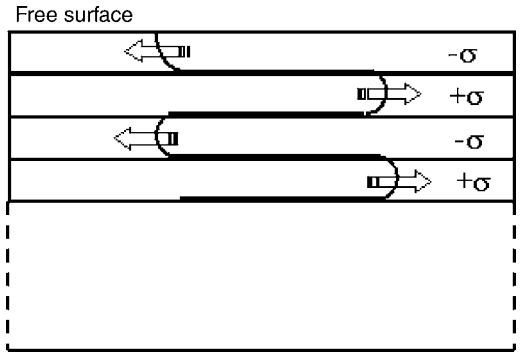

FIG. 2. Schematic illustrating the glide of a threading dislocation in different layers.

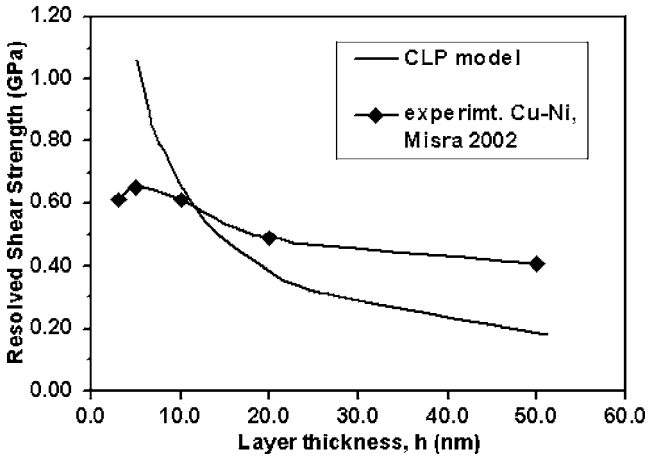

FIG. 3. Comparison between the strength predictions of the classical confined layer plasticity model with experimental results for Cu/Ni system (Ref. 11).

wake two dislocations, one at each interface, which results in the well-known hairpin configuration, Fig. 2. This process is commonly referred as Orowan bowing and the stress required to propagate a threading dislocation in this confined fashion is commonly referred to as the *channeling stress*.[14] As well established, the prediction of the channeling stress based on the Orowan bowing of single dislocation in a rigid channel model significantly underestimates the strength of NMM composites. In real systems, one expects that a threading dislocation will interact with other existing dislocations including threading dislocations and interfacial dislocations on parallel and/or intersection planes. In this work, we use DD analysis to investigate the contribution of the interaction between a threading dislocation and orthogonal interfacial dislocations to the increased strength measured in real systems.

Analytical models, for the onset of confined layer plasticity (CLP) by the glide of threading dislocations, were developed by Frank and van der Merwe[15] and Matthews and Blakeslee.[12] Historically, these models were developed to predict the critical thickness at which interfacial dislocations are generated in heterogeneous epitaxial semiconductor films and layers. During the growth of coherent multilayered structures, mismatch between the lattice parameters of the two materials results in a biaxial misfit stress in the layers and hence elastic energy stored in the structure, which increases linearly with thickness as the layer grows thicker. At a certain critical thickness it becomes energetically favorable for the system to relax part of the misfit strain by nucleating dislocations, thus trading elastic energy for defect energy. The same physical concept governs the determination of the channeling stress of a threading dislocation for a given layer thickness. From a mechanistic point of view,[12] the idea is based on the balance between the force exerted by the misfit stress on the threading dislocation and the tension force in the created dislocation lines. For a certain critical layer thickness, h_c, the two forces become equal and the threading dislocation becomes unstable and propagates. By equating those forces, one finds the channeling stress dependence on layer thickness to be proportional to $\ln(h)/h$, h being the layer thickness. The same concept can also be considered from an energetic point of view leading to the same result.[13,16,17] This simple model, however, underestimates the measured strength of NMM composites. Figure 3 is a compilation of the predictions of this classical model (the CLP model) for the channeling stress and experimentally measured strength of Cu/Ni cube-on-cube system with {100} interface orientation. The fact that both Cu and Ni are fcc metals, and have low lattice parameter mismatch and a small difference in elastic properties, makes this system well-suited for comparison to simple starting-point models before further complexity associated with general real systems is included. As can be seen from the figure, the measured strength is higher with the gap increasing with increasing layer thicknesses. Suggested explanations for this discrepancy again came historically from observations regarding the relaxation process of misfit strain and the corresponding critical thickness. The observation that the fraction of misfit strain relaxed by dislocations is much lower than that predicted for a given system and layer thickness indicates that significant impediment to dislocation propagation must exist in real systems. Among the proposed reasons for this impediment include dislocation-dislocation interactions leading to work hardening, barriers to dislocation nucleation, kinetic effects,[18] Peierls friction stress,[19] and step formation at surfaces and interfaces.[20] To complete the general picture drawn in Fig. 3, the saturation and eventual dropping of the strengthening effect represent other important issues which have yet to be understood. Theories put forward to explain the latter effects tie the point of saturation to the breakdown of the confining effect due to the interface acting as a barrier to dislocation crossing from one layer to the other.[11]

The above-mentioned models for dislocation threading consider the introduction, in an otherwise defect-free medium, of a single dislocation dipole. In a real system, however, the threading of many dislocations in the form of orthogonal arrays will occur. Based on this observation, several authors developed energy expressions for stable dislocation arrays in multilayered systems as a function of layer thickness.[21–27] These approaches are more realistic—and resulted in enhanced predictions for the critical layer thickness for the onset of dislocation generation in multilayered structures. However, they assume simplified configurations for intersecting dislocations and perforce give approximate re-

Downloaded 03 Nov 2009 to 128.12.160.33. Redistribution subject to AIP license or copyright; see http://jap.aip.org/jap/copyright.jsp

sults. The same applies for the calculations made by Freund[28] and Nix[14] for the blocking effect an orthogonal interfacial dislocation and an array of them, respectively, has on a threading dislocation. The use of DD modeling gives an improved analysis of local configurations and should give an improved relationship for the effect of layer thickness on strength.

In DD analysis actual dislocation structures with complex geometry are explicitly treated by the direct calculation of the Peach-Koehler force exerted on a dislocation by all existing stress fields, including those of the dislocations themselves, followed by the advancement and updating of dislocation positions using a physical mobility law. Other long-range effects from different boundary conditions can also be accounted for through the multiscale finite element (FE) and DD coupling. To the extent to which the short reaction rules used are physical, DD analysis can also capture dislocation-dislocation interactions including junction formation, annihilation, and cross slip; all of which are critical to any realistic predictions. When large systems consisting of many dislocations, applied loads, and various boundary conditions are dealt with, DD coupled with FE can handle this complexity simultaneously. For complete details on the DD analysis and its coupling with FE, the reader is referred to Refs. 29 and 30, which provide a comprehensive overview of the topic.

Published DD analyses of nanoscale multilayers are limited. Pant *et al.*[31] studied dislocation interactions in layers with impenetrable walls, and found that the blocking effect an intersecting interfacial dislocation has on a threading dislocation is weak, contrary to the predictions of simple analytical models.[11,14,28] Considering all four possibilities of orthogonal encounters between interfacial dislocations and a threading dislocation in (001) and (111) Cu films, they observed interactions that were either junction formation (two cases) or annihilation (one case), while the fourth case, involving the interaction between the $(1\bar{1}1)[011]$ threading dislocation and the $(111)[0\bar{1}1]$ interfacial dislocation, did not result in a junction (nor annihilation). Furthermore, junction formation was found to depend on layer thickness: the thinner the film, the greater the channeling stress, which in turn leads to the interfacial dislocations being pushed so strongly against the impenetrable interfaces to the point where they can no longer move locally and reorient themselves so as to engage in short-range reactions. The maximum increase in the channeling strength for an 800 nm thick layer was found to be about 20% for the no-junction case, 10% for the junction formation case with the effect being stronger for thicker layers, while for the annihilation case the strengthening effect was 16%. In another effort, DD analysis of the blocking effect of a single fixed (nonreacting) interfacial dislocation[32] found that the maximum strengthening effect above the unobstructed channeling stress was 15%, much less than the corresponding analytical result of 50%.[28] The suggested reason for this discrepancy was that, in DD calculations, the threading dislocation can dynamically adjust its configuration so as to bypass the obstacle with minimum resistance. The same problem addressed in Ref. 32 was revisited (using DD) but with the interfacial dislocation free to move and react while being confined to its layer by a stress-free neighboring layer.[33] The blocking effect was found to be even weaker than that found in the fixed dislocation case[32] because the interfacial dislocation could now be locally pushed into the stress-free layer offering less resistance than a rigid interface, hence presenting less restriction on the threading dislocation. As reported, even if a small restoring stress is applied to the neighboring layer, the strengthening effect is never above 15%.

Hence, a few DD analyses with a limited number of dislocations[31–33] have indicated that the predicted strengthening can differ markedly from the simple analytical results. In this work, we use a more extensive DD analysis to examine the strengthening effect due to the interaction between threading dislocations and intersecting interfacial dislocations. First, we obtain DD predictions for the channeling stress in a rigid channel, and compare them to the results of the classical CLP model as well as with a complete energetic model, which was developed for validation purposes. Using flexible boundary conditions for layer interfaces, we then investigate the reactions resulting from the intersection of

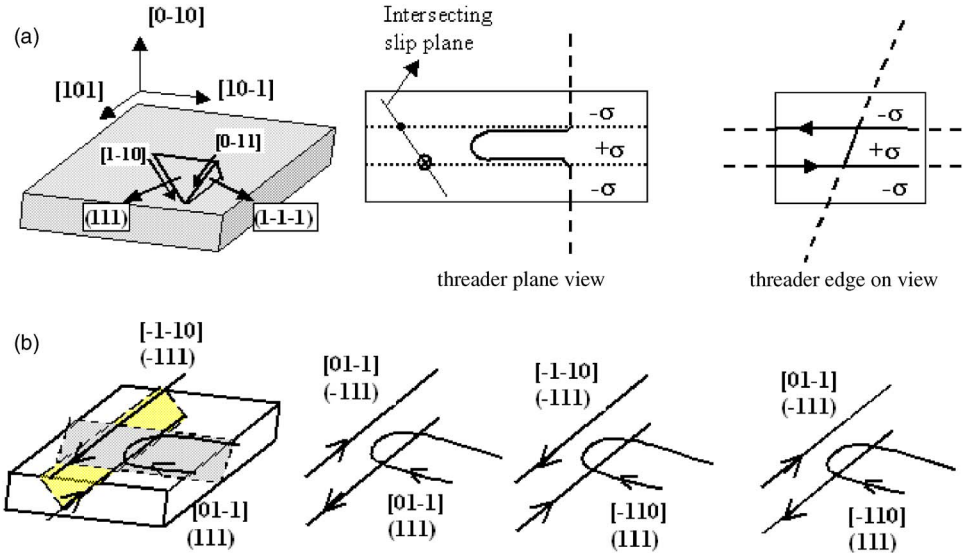

FIG. 4. Problem setup; (a) crystallographic orientation of the layers idealized setup; (b) four encounters representing all possible intersections between threading dislocation and $a/2\langle 011\rangle$-type interfacial dislocation dipoles.

Downloaded 03 Nov 2009 to 128.12.160.33. Redistribution subject to AIP license or copyright; see http://jap.aip.org/jap/copyright.jsp

TABLE I. Physical properties of Cu used in DD calculations.

Density (kg/m^3)	8980.0
Burgers vector magnitude (Å)	2.556
Shear modulus (GPa)	38.46
Poisson's ratio	0.3
Core size (b: Burgers' vector magnitude)	1.0
Mobility (1/Pa s)	1.0×10^4

different combinations of threading and interfacial dislocations and their strengthening effects. Climb, as a possible relaxation mechanism, is not considered in this analysis.

II. PROBLEM SETUP IN DD

Figure 4 shows the problem setup and crystallography. A three-layered Cu system is used to idealize confined layer slip in a coherent multilayer system with small lattice parameter mismatch and moderate elastic properties difference, as in a {001} Cu/Ni cube-on-cube system. Table I lists the physical properties of Cu used in the model. The initial configuration consists of an $a/2\langle011\rangle$ threading dislocation residing on a (111) slip plane in the middle layer, as well as a long, orthogonal $a/2\langle011\rangle$ interfacial dislocation dipole residing on the $(\bar{1}11)$ plane. This interfacial dipole can be thought of as resulting from an earlier threading event on a $(\bar{1}11)$ plane. In accordance with the fundamental principle of continuity of dislocation lines, two fixed semi-infinite dislocation lines, with the same line sense as that of the threading dislocation segment, are attached to both ends. Dislocations in the middle layer are driven by the application of biaxial tensile stress of a desired magnitude in this layer. In the bounding layers, a biaxial compressive stress equal in magnitude to that applied in the middle layer is applied. As in coherent or semicoherent systems, the effect of this stress is to confine dislocations initially in the middle layer to that layer. With these flexible boundary conditions, interfacial dislocations are not overconstrained, as in the case of impenetrable boundaries, because, although confined to their layer, they can still move locally to adjust their configuration in response to the stress state. This in turn allows for the possibility of short-range interactions upon the encounter of the threading dislocation with the interfacial dislocations. Restricted by slip crystallography, four representative encounters between threading dislocations and intersecting interfacial dislocations are possible (see Fig. 4).

Nanoscale composites represent an unconventional application for DD analysis. While typical DD applications involve microscale specimens and dislocation segments on the order of 100 b, the layer thickness range of interest in our case can be as small as 25 b and up to 500 b. This requires the use of discrete segment lengths on the order of a few b's. The stress, of the order of several gigapascal, needed to drive dislocations confined to nanolayers requires the use of suitably small time steps. Both the spatial and temporal discretizations in this problem require optimization for stability and accuracy. An optimized mean segment length of 3.5 b was used in these simulations: however, the actual segment length is locally decided, based on the dislocation line curvature, by an adaptive meshing technique.[29] The choice of the time step is also automated based on dislocation velocities and the detected possibility of short-range interactions.[29] Table II lists the main numerical parameters used in the DD simulation. Originally, the core was optimized as a numerical parameter to match the force calculations from an exact analytical model for a corresponding problem.[34] Here instead, the core size was fixed as 1 b and the average force per unit length on a given dislocation segment from its neighboring segment is calculated from the following equation, which is equivalent to an earlier expression for the case of an adjustable core size:[34]

TABLE II. Main numerical parameters used in DD calculations. Within the minimum and maximum segment length, the precise choice is made automatically based on adaptive meshing.

Mean segment length (b)	3.5
Minimum segment length (b)	1.75
Maximum segment length (b)	5.25
β parameter [Eq. (1)]	0.5
Time step (s) (variable)	$1.0\times10^{-13}-3.0\times10^{-13}$

$$\left(\frac{F}{L}\right)_{\text{avg}} = \frac{\mu}{4\pi L} f_1(\theta,b)\left[\left(\ln\left(\frac{L}{b}\right)+\beta\right)\right], \tag{1}$$

where $(F/L)_{\text{avg}}$ is the average force per unit length acting on a dislocation segment of length L, μ is the shear modulus, $f_1(\theta,b)$ is a functional multiplier given in Ref. 35, p. 138, and β is an adjustable parameter that compensates for the energy contained in the core size. To validate our choice of parameters, a complete energetic model for the threading process in a rigid channel is developed and its results, as well as those of the classical CLP model, are compared to DD results. Here, "complete" means that the inherent assumptions to the CLP model, infinite dipole length, and the layer thickness as the external cutoff radius in the logarithmic term in the energy expression, are relaxed. The Appendix describes the details of the model and the comparison results, which strongly validate the DD model for confidence in its results in more complex situations.

III. RESULTS AND DISCUSSION

The four representative cases for the intersection encounters between threading dislocations and glide interfacial dislocations are shown in Fig. 4. Table III lists these interactions and their energetic favorability. Consistent with these trends, annihilation reaction is observed in the DD simulation for case 1 at both the lower and upper interfaces where interfacial dislocations reside. For the threading dislocation to overcome the obstacle (i.e., the interfacial dipole) and the threading process to continue, the annihilation process needs to occur twice. Figures 5(a)–5(d) show this process and the corresponding dislocation configuration in the intermediate stages. As shown in Fig. 6, which is a close-up of the annihilation reaction occurring within circled region in Fig. 5(b), the interaction involves a complex process of local realignment of the interfacial and threading dislocations to produce a configuration that is admissible to an annihilation reaction.

Downloaded 03 Nov 2009 to 128.12.160.33. Redistribution subject to AIP license or copyright; see http://jap.aip.org/jap/copyright.jsp

TABLE III. Possible encounters between threading and $a/2\langle 011\rangle$ type interfacial dislocations on intersecting planes and the corresponding reactions.

Case no.	Reactants		Reaction favorability		Expected reaction
	Threading dislocation	Interfacial dislocation	Parallel sense	Antiparallel sense	
1	$a/2[01\bar{1}]$; (111)	$a/2[01\bar{1}]$; $(\bar{1}11)$	Neutral	Favorable	Annihilation
2	$a/2[01\bar{1}]$; (111)	$a/2[\bar{1}\bar{1}0]$; $(\bar{1}11)$	Favorable	Unfavorable	Junction formation
3	$a/2[\bar{1}10]$; (111)	$a/2[01\bar{1}]$; $(\bar{1}11)$	Unfavorable	Favorable	Junction formation
4	$a/2[\bar{1}10]$; (111)	$a/2[\bar{1}\bar{1}0]$ $(\bar{1}11)$	Neutral	Neutral	Junction formation

This configuration consists of two antiparallel screw-oriented segments, each belonging to a different dislocation, and attracting each other to a common position along the line of intersection of the two slip planes. After this configuration is achieved, Fig. 6(c), the annihilation process occurs, leaving behind two dislocation nodes *i* and *j*, which can move only along the line of intersection of slip planes, Fig. 6(d). Notice that a 90° dislocation bend structure has resulted from the joining of the trailing arm of the threading dislocation at the lower interface with that part of the interfacial dislocation at the lower interface which maintains the line sense of the aforementioned part of the threading dislocation, Figs. 5(b)–5(d) and 6(d). This dislocation structure has been observed experimentally at the interfaces in NMM composites (e.g., see the TEM images in Ref. 36). The above observation, that dislocations with initially repulsive interaction readjust their configuration to reach a minimum energy configuration involving annihilation, was also made by Madec *et al.*[37]

Table IV(a) details the incremental strengthening effect of the two annihilation reactions as a function of layer thickness. The third column in this table indicates the increase in stress, above that of the unobstructed threading case listed in column 2, necessary to push the threading dislocation against the long-range stress field of the interfacial dislocation dipole, as close as possible to it, yet not close enough to overcome the repulsive force and interact. In the simulation, this stress was noted after allowing the simulation to run long enough at that stress without observing the first annihilation reaction. The additional stress needed to push the threading dislocation beyond the first interfacial dislocation by inducing the annihilation reaction, fourth column in Table IV(a), is due to the activation energy to reorient the dislocation segments for annihilation. If the stress is not increased further, the new dislocation configuration, Fig. 5(b), remains unchanged. To push the dislocation ahead from this position, another increase in stress is needed. Although a small portion of the original threading configuration is lost upon the first annihilation interaction, the new connection to the interfacial dislocation has a high curvature, resulting in higher line tension and leading to higher resistance to further threading. Another contribution to this hardening effect is that, as in the first reaction, energy needs to be spent to perform the realignment necessary for the reaction to take place. The same behavior is observed for the case of a single $a/2\langle 011\rangle$ interfacial dislocation acting as the obstacle to threading. Obviously, only one annihilation reaction occurs. Table IV(b) breaks down the strengthening effect due to each of the three stages of the bypass process for this case: (a) bowing out of the threading dislocation to closely approach the interfacial dislocation just before the reaction is induced, column 3; (b) annihilation reaction leaving behind a configuration similar to that in Fig. 5(b) (except for the absence of the interfacial dislocation at the upper interface), column 4; and (c) the final stage of completely overcoming the obstacle and the resumption of the threading process, column 5. If the stress value shown in column 4 of Table IV(b) is applied without further increase, the threading dislocation will only perform the annihilation and get stuck at that point. Similarly, if only the stress level shown in column 3 is applied and no more, the threading dislocation will be arrested close to the interfacial dislocation and will not advance any further. A comparison of the strengthening effect due to a single and a dipole $a/2\langle 011\rangle$ interfacial dislocation obstacle for any corresponding bypassing stages, Tables IV(a) and (b), indicates that the presence of the second interfacial dislocation in the dipole contributes to a higher resistance at all stages. Furthermore, the strengthening effect due to this interaction (dislocations with collinear Burgers' vectors on intersecting slip planes)

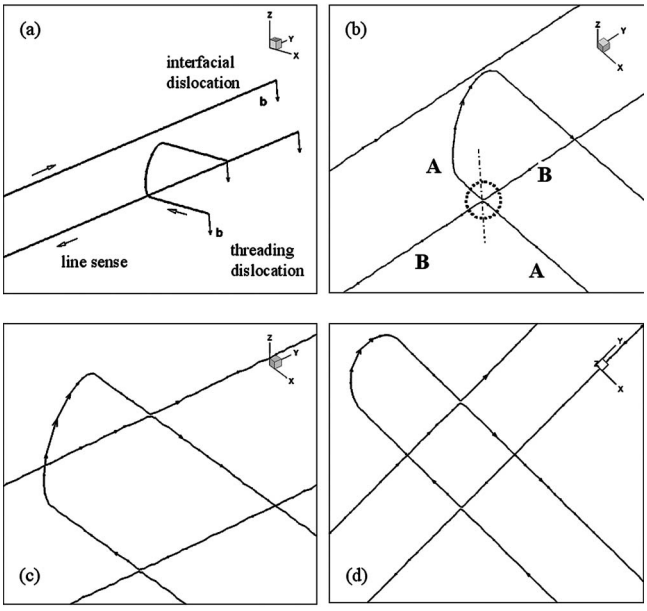

FIG. 5. Stages of interaction between $a/2[01\bar{1}](111)$ threading and $a/2[01\bar{1}](\bar{1}11)$ interfacial dislocation; (a) arrest of threading dislocation by the long-range stress field of the interfacial dislocation; stress needs to be increased to propagate further; (b) intermediate configuration after first annihilation reaction at lower interface (circled region indicates region zoomed-in at in Fig. 6); (c) final configuration after second annihilation at upper interface; (d) interface plane view of final dislocation configuration.

Downloaded 03 Nov 2009 to 128.12.160.33. Redistribution subject to AIP license or copyright; see http://jap.aip.org/jap/copyright.jsp

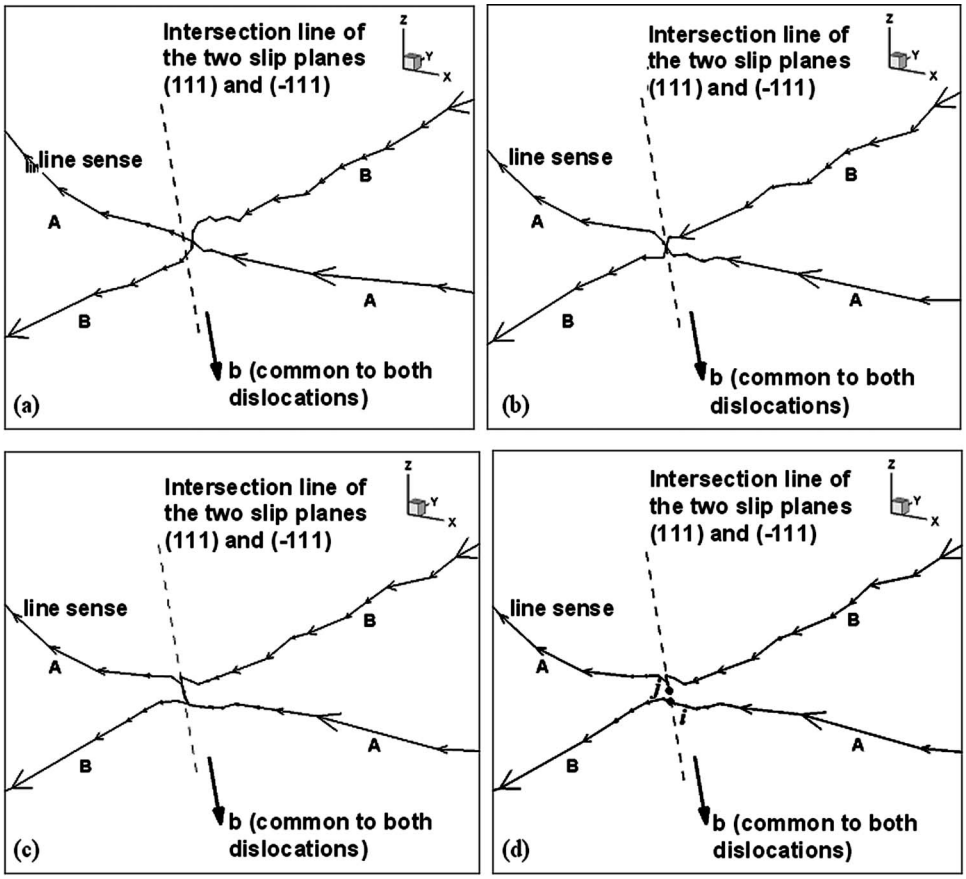

FIG. 6. Sequence of DD snapshots showing the details of the realignment process which the $a/2[01\bar{1}](111)$ threading dislocation A and the $a/2[01\bar{1}](\bar{1}11)$ interfacial dislocation B undergo leading to the annihilation reaction.

was found to be the strongest among other possible interactions. The same conclusion was made from large-scale DD simulations of forest interactions in fcc crystals.[37]

Figure 7 summarizes the DD predictions, based on the three-layer model, for the channeling stress in the absence and presence of $a/2\langle 01\bar{1}\rangle$ single and dipole interfacial dislocations intersecting the path of a threading dislocation with the same Burgers' vector. When an interfacial dislocation(s) exits, the channeling stress, i.e., the minimum stress needed for the threading dislocation to completely overcome the obstacle and continue past it, has the values reported in column 5 in Tables IV(a) and (b). Also shown in the same plot are

TABLE IV. (a) Strengthening effect of annihilation reactions between $a/2[01\bar{1}](111)$ threading dislocation and $a/2[01\bar{1}](11\bar{1})$ interfacial dipole as a function of layer thickness. (b) Strengthening effect of annihilation reactions between $a/2[01\bar{1}](111)$ threading dislocation **and** $a/2[01\bar{1}](\bar{1}11)$ single interfacial dislocation as a function of layer thickness.

(a) Layer thickness (nm)	Reference (no obstacle) strength τ_o [a] (GPa)	Stress to approach obstacle, just before reacting (τ/τ_o)	Stress to overcome first dislocation in the interfacial dislocation dipole (τ/τ_o)	Stress to overcome second dislocation and completely bypass the dipole (τ/τ_o)
6.4	1.04	1.06	1.10	1.13
12.8	0.57	1.14	1.21	1.51
19.2	0.41	1.20	1.29	1.59
25.6	0.31	1.32	1.45	1.58
51.1	0.16	1.25	1.50	1.66

(b) Layer thickness (nm)	Reference (no obstacle) strength τ_o [a] (GPa)	Stress to approach obstacle, just before reacting (τ/τ_o)	Stress to overcome the interfacial dislocation by inducing annihilation reaction (τ/τ_o)	Stress to bypass the interfacial dislocations and resume threading (τ/τ_o)
6.4	1.04	1.04	1.06	1.26
12.8	0.57	1.11	1.15	1.29
19.2	0.41	1.05	1.10	1.29
25.6	0.31	1.05	1.19	1.58
51.1	0.16	1.28	1.35	1.48

[a]Strength values are as resolved on the slip system.

Downloaded 03 Nov 2009 to 128.12.160.33. Redistribution subject to AIP license or copyright; see http://jap.aip.org/jap/copyright.jsp

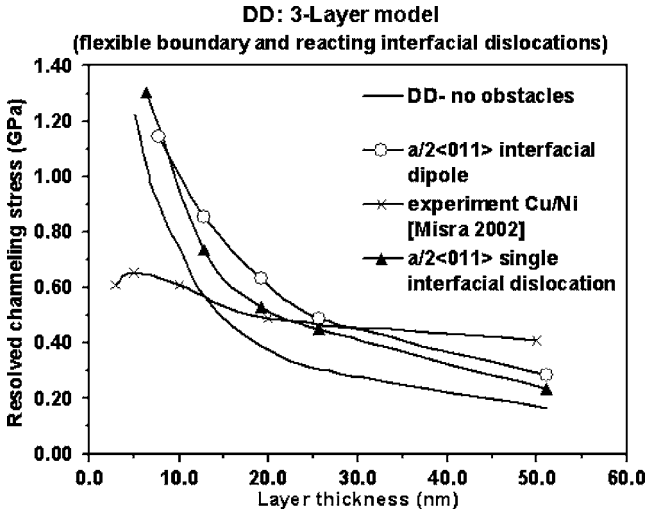

FIG. 7. Comparison of measured strength of Cu/Ni bimetallic system (Ref. 11) with DD predictions using the three-layer idealized model (flexible confinement boundary conditions and reacting interfacial dislocations). The strengthening effect is due to annihilation reactions occurring between a threading dislocation and an intersecting interfacial dislocation of the same Burgers' vector.

the experimental results for the strength of Cu/Ni multilayered system previously shown in Fig. 3. Thus, including the interactions of a threading dislocation with orthogonal interfacial dislocations, as expected to happen frequently in a real system, does bring the baseline DD predictions (threading without obstacle) closer, yet not matching, to the experimental measurements for layer thicknesses of 30 nm and above. However, the three-layer model overestimates the strength below this range, as does the CLP model. This indicates that orthogonal intersections between threading dislocations and interfacial dislocations cannot be considered as the single dominant mechanism to account for the discrepancy between the experiment and the model. Obviously, deformation mechanisms in actual systems are more complicated and multiple in nature. Mechanisms such as interface crossing, which are softening in nature, play an important role in the 30 nm and below range and cannot be ignored. This conclusion supports a similar general one made by Pant[31] on the existence of different mechanisms at different length scales. Also, other mechanisms could be important with larger misfits, and with different crystal structures for the two types of layers.

For the other cases of intersections where a junction forms upon interaction, the threading process ceases, as long as no other conditions, e.g., load reversal, arise to unzip the junction and free the threading dislocation. DD analyses reporting on junction formation under different boundary conditions from the ones used here indicate that the strength is weaker and annihilation remains the stronger reaction.[31] Other mechanisms, such as cross slip, as well as long-range effects in systems with many dislocations, play an important role in determining strength. Those issues are the subject of a forthcoming article in which results from massive DD analyses will be reported.[38]

Finally, we examined the effect of the assumption of rigid channel walls on the threading process. DD analysis for

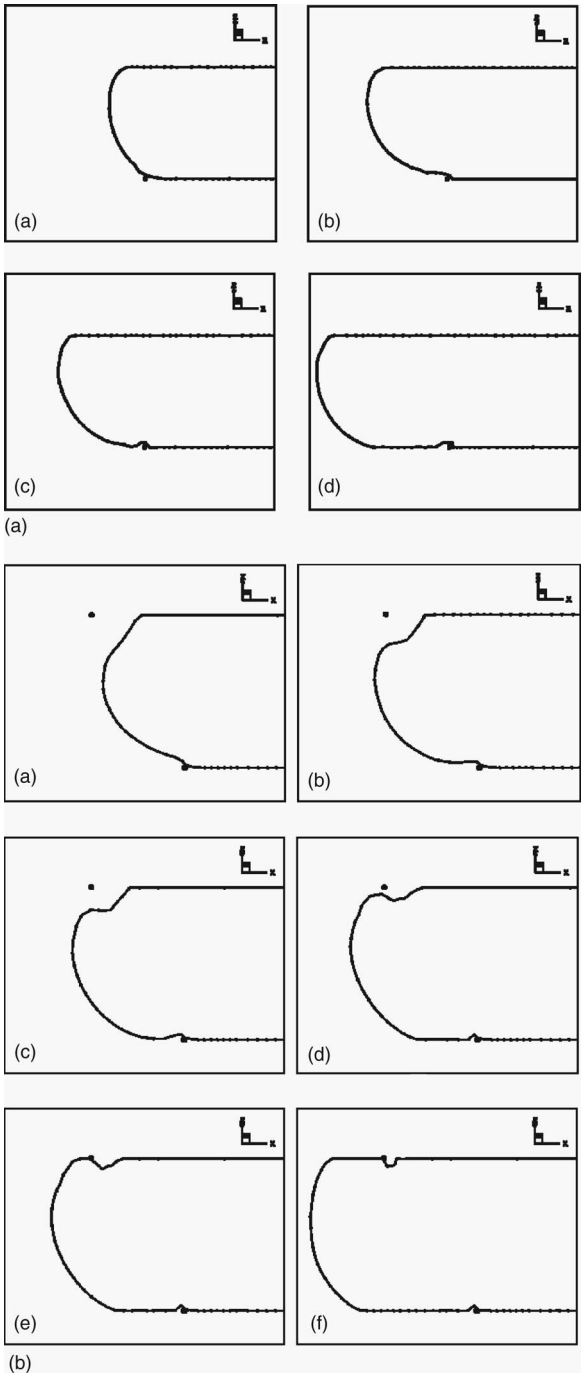

FIG. 8. (a) Slip plane (111) view of a sequence of DD snapshots of the bypassing process of $a/2[01\bar{1}](111)$ threading dislocation over a Lomer-type interfacial dislocation with Burgers' vector $a/2[10\bar{1}]$ (globally, parallel to the x-axis) in a 13 nm thick layer under a stress of 1.7 GPa. (b). Slip plane (111) view of a sequence of DD snapshots of the bypassing process of $a/2[01\bar{1}](111)$ threading dislocation over $a/2[01\bar{1}](\bar{1}11)$ interfacial dislocation dipole treated as pinned and nonreacting in a 13 nm thick layer under a stress of 2.1 GPa.

the interaction of an $a/2[01\bar{1}](111)$ threading dislocation with $a/2[01\bar{1}](\bar{1}11)$ single and dipole interfacial dislocations as well as with Lomer-type interfacial dislocation was performed under the assumption of rigid channel walls with pinned dislocation. The first two cases correspond to those studied using the three-layer model and whose results are presented in Tables IV(a) and (b) and Fig. 7. Figure 8 shows a sequence of DD snapshots of the bypassing process of the

Downloaded 03 Nov 2009 to 128.12.160.33. Redistribution subject to AIP license or copyright; see http://jap.aip.org/jap/copyright.jsp

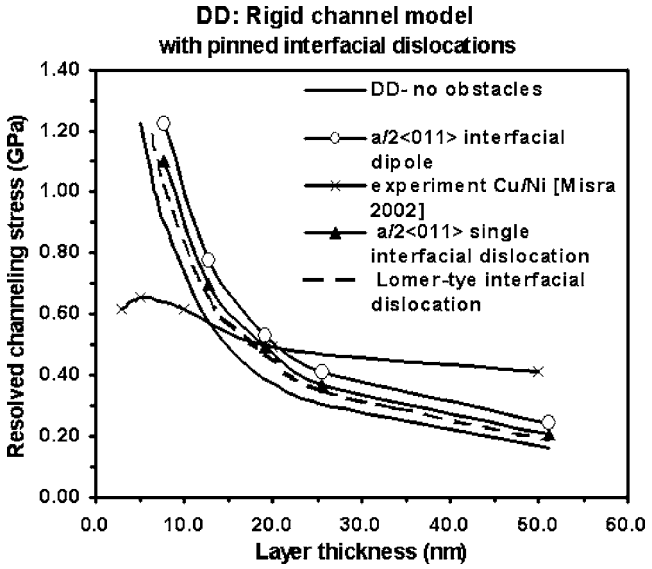

FIG. 9. Comparison of measured strength of Cu/Ni bimetallic system (Ref. 11) with DD predictions using the rigid channel idealized model (impenetrable layer interfaces and pinned interfacial dislocations). The strengthening effect is due to annihilation reactions occurring between a threading dislocation and an intersecting interfacial dislocation of the same Burgers' vector.

threading dislocation in two cases: (a) over a Lomer-type interfacial dislocation, and (b) through an interfacial dislocation dipole representing the two arms deposited in the wake of a threading dislocation. A third case, bypassing over an $a/2\langle 011\rangle$ type interfacial dislocation, was also performed and the sequence was found to be similar to that of the Lomer-type case; thus, it is not included here for brevity. As can be deduced from the figure, there is a sequence of complex, dynamically changing configurations for the threading dislocation during the bypassing process, and the notion of a critical effective thickness through which the threading dislocation passes[28] is not well defined. Another difference between the rigid channel model with pinned interfacial dislocations and the flexible boundary results is in the predictions of the strengthening effect. Figure 9 shows DD predictions, for the case of the rigid channel model with pinned interfacial dislocation, for the channeling stress in the absence and presence of $a/2\langle 01\bar{1}\rangle$ single and dipole interfacial dislocations intersecting the path of a threading dislocation with the same Burgers' vector (same cases used to generate Fig. 7). Also shown in the figure are the Cu/Ni measured strength values[11] and the strengthening effect due to a Lomer-type interfacial reaction. As can be seen by comparing Figs. 7 and 9, which are plotted using the same scale for the ease of comparison, the strength predictions of rigid channel with pinned interfacial dislocations underestimate the strength of NMM composites when compared to the more realistic three-layer model predictions and more so when compared to the experimental results.

IV. CONCLUSIONS

- The use of flexible dislocations (which allows for short-range interactions) and flexible channel walls (where dislocations are confined by coherency stress) leads to an improved agreement between predicted and experimentally measured strengths in nanoscale multilayered composites.
- Among the possible interactions between threading and orthogonal interfacial dislocations, the strongest contributor to hardening is that involving dislocations of collinear Burgers' vector. For this case, the bypassing process entails annihilation reactions and leaves behind a 90° bend dislocation structure. In the thickness range of 10–50 nm, the increased strength due to this interaction is about 1.5 times the reference (free threading with no obstacles present) strength.

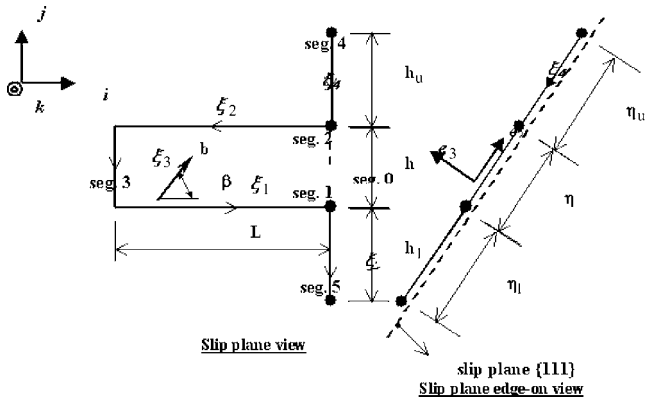

FIG. 10. Dislocation configuration modeling the threading process in a confined layer.

ACKNOWLEDGMENT

This research is sponsored by the U.S. DOE, Office of Science, Office of Basic Energy Sciences.

APPENDIX: ENERGETIC MODEL FOR CHANNELING STRENGTH

Figure 10 outlines the main features of the energetic model used to estimate the channeling strength of a threading dislocation. The initial configuration consists of an infinite dislocation line, here made of a finite segment 0 and two semi-infinite segments 4 and 5. As the side view shows, the dislocation resides on a {111} slip plane and the crystallographic setup corresponds to that in Fig. 4. Segment 0 represents the part of the dislocation which will bow out into a hairpin confined to the layer of thickness h under the effect of the applied stress. The semi-infinite segments are a necessity to maintain the dislocation continuity. A stress is applied to the layer, with τ representing its resolved shear component in the slip plane along the Burgers' vector. Under the effect of this applied stress, the threading dislocation advances, segment 3, depositing two finite misfit dislocations of length l, segments 1 and 2. The change of the system configuration energy ΔW as follows:

$$\Delta W = W(l,h) = \begin{pmatrix} 2W_1 + W_3 + 2W_5 + W_{12} + W_{31} + W_{32} \\ + 2W_{35} + W_{15} + W_{42} + W_{52} + W_{14} + W_{45} \end{pmatrix} - (W_0 + 2W_5 + 2W_{05} + W_{45}). \quad \text{(A1)}$$

Downloaded 03 Nov 2009 to 128.12.160.33. Redistribution subject to AIP license or copyright; see http://jap.aip.org/jap/copyright.jsp

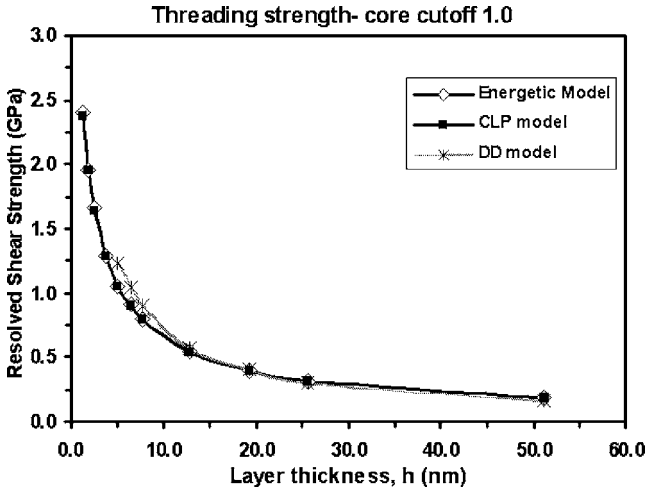

FIG. 11. Critical stress for threading in a confined rigid channel of thickness h, comparison of different models' predictions: classical CLP model, DD models, and our energetic model.

W with a single subscript represents a self-energy, while that with two subscripts represents the interaction energy between the two segments indicated by the two subscripts. All the expressions needed for self- and interaction energies can be found in Ref. 35. The final result for the ΔW expression is a function of h and l and, after some algebra, reduces to (to avoid the infinite energies of the semi-infinite segments, the terms W_{35} and W_{05} should be considered simultaneously, series expansion performed on the combined expression, and second term in the expansion kept)

$$\Delta W = 2C_0 L \ln\left(\frac{L}{e\rho}\right) + C_1\left\{2\eta - 2\sqrt{l^2+\eta^2} + 2l\ln\left(\frac{\sqrt{l^2+\eta^2}+l}{\eta}\right)\right\} + C_{10}\left\{\sqrt{l^2+\eta^2} + \eta\ln\left(\frac{2\eta}{\sqrt{l^2+\eta^2}+\eta}\right) - l - \eta\right\}, \tag{A2}$$

$$C_0 = \frac{\mu b^2}{4\pi}(\cos\beta)^2 + \frac{\mu b^2}{4\pi(1-\upsilon)}(\sin\beta)^2,$$

$$C_1 = -\frac{\mu b^2}{4\pi}(\cos\beta)^2 - \frac{\mu b^2}{4\pi(1-\upsilon)}(\sin\beta)^2,$$

$$C_{10} = \frac{\mu}{4\pi}(\sin\beta)^2 + \frac{\mu b^2}{4\pi(1-\upsilon)}(\cos\beta)^2. \tag{A3}$$

The equilibrium position of the threading dislocation corresponding to a certain applied stress can be determined by minimizing the free energy, $\Delta G = \Delta W - \tau b \eta l$, while the stable point beyond which the threading dislocation propagates indefinitely can be determined for a given layer thickness h from the condition $\partial^2 \Delta G / \partial l^2 = 0$. Figure 11 shows the results of performing those calculations for the critical channeling stress as a function of layer thickness, expressed in terms of its resolved shear component, which satisfies both conditions. Physically, this stress corresponds to the stress needed to bow out the threading dislocation to the point

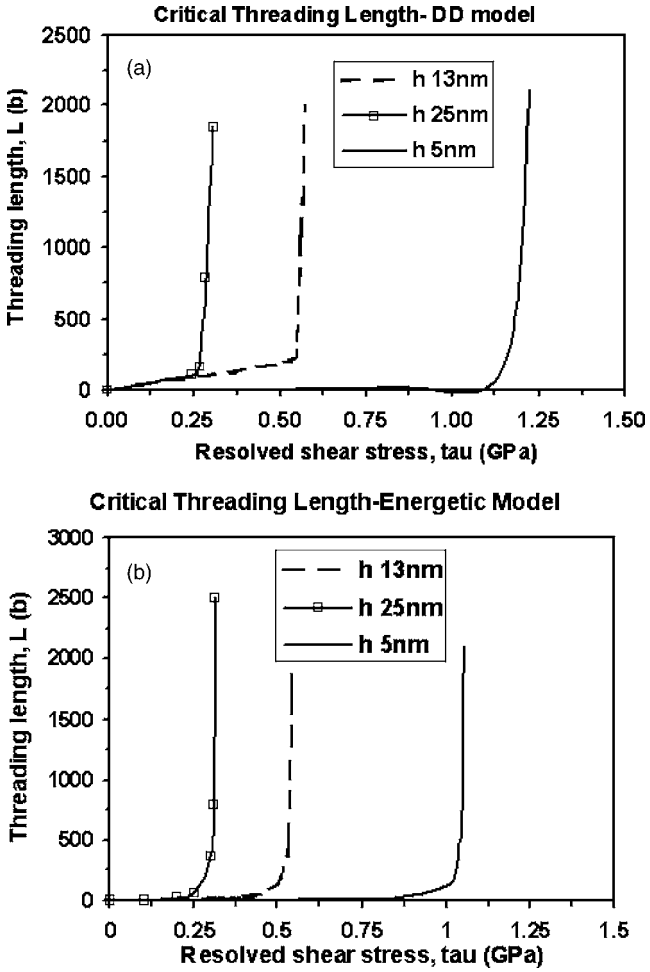

FIG. 12. Threading length as a function of applied stress, comparison between DD model and our energetic model. The CLP model only predicts infinite threading once the applied stress reaches a critical value.

where the hairpin configuration is not stable anymore and the dislocation will propagate indefinitely. At any stress value below this critical stress the dislocation will bow out to a certain equilibrium length proportional to the applied stress. For comparison and validation purposes, the channeling stress prediction from the classical CLP model and the prediction of our DD model are shown in Fig. 11. As can been seen from the figure, our DD model produces excellent agreement with the analytical models. Furthermore, our energetic model and the CLP model match perfectly as far as the stress prediction is concerned, in spite of the fact that the CLP model starts out by assuming semi-infinite arms connected to the threading dislocation and finding their dipole energy by taking the external cutoff radius in the logarithmic term of the energy expression to be equal to the layer thickness. Our energetic model remains more complete because it considers the exact configuration and includes all the interaction energies, and is physically based on minimizing the free energy of the system. This principle difference reflects in the fact that our energetic model predicts an equilibrium threading length for any applied stress below the critical stress, while the CLP model does not. In this regard, DD calculations support this finding of our energetic model predictions. Figure 12 shows the agreement between the DD model and our energetic model in this regard.

Downloaded 03 Nov 2009 to 128.12.160.33. Redistribution subject to AIP license or copyright; see http://jap.aip.org/jap/copyright.jsp

[1]A. Misra and H. Kung, Adv. Eng. Mater. **3**, 217 (2001).
[2]M. Shinn and S. A. Barnett, Appl. Phys. Lett. **64**, 61 (1994).
[3]G. S. Was and T. Foecke, Thin Solid Films **286**, 1 (1996).
[4]B. M. Clemens, H. Kung, and S. A. Barnett, MRS Bull. **24**, 20 (1999).
[5]R. R. Oberle and R. C. Cammarata, Scr. Metall. Mater. **32**, 583 (1995).
[6]A. Misra, X. Zhang, D. Hammon, and R. G. Hoagland, Acta Mater. **53**, 221 (2005).
[7]N. Mara, A. Sergueeva, A. Misra, and A. K. Mukherjee, Scr. Mater. **50**, 803 (2004).
[8]Y. C. Wang, A. Misra, and R. G. Hoagland, Scr. Mater. **54**, 1593 (2006).
[9]M. R. Stoudt, R. E. Ricker, and R. C. Cammarata, Int. J. Fatigue **23**, 215 (2001).
[10]T. Höchbauer, A. Misra, K. Hattar, and R. G. Hoagland, J. Appl. Phys. **98**, 123516 (2005).
[11]A. Misra, J. P. Hirth, and H. Kung, Philos. Mag. A **82**, 2935 (2002).
[12]J. W. Matthews and A. E. Blakeslee, J. Cryst. Growth **27**, 118 (1974).
[13]J. W. Matthews, in *Dislocations in Solids*, edited by F. R. N. Nabarro (North-Holland, Amsterdam, 1979), Vol. 2, pp. 461–545.
[14]W. D. Nix, Scr. Mater. **39**, 545 (1998).
[15]F. C. Frank and J. H. van der Merwe, Proc. R. Soc. London, Ser. A **198**, 205 (1949).
[16]W. D. Nix, Metall. Trans. A **20A**, 2217 (1989).
[17]L. B. Freund, J. Appl. Mech. **54**, 553 (1987).
[18]B. W. Dodson and J. Y. Tsao, Appl. Phys. Lett. **51**, 1325 (1987).
[19]J. W. Matthews, S. Mader, and T. B. Light, J. Appl. Phys. **41**, 3800 (1970).
[20]R. G. Hoagland, R. J. Kurtz, and C. H. Henager, Jr., Scr. Mater. **50**, 775 (2004).
[21]X. Feng and J. P. Hirth, J. Appl. Phys. **72**, 1386 (1992).
[22]J. P. Hirth and X. Feng, J. Appl. Phys. **67**, 3343 (1990).
[23]T. J. Gosling, J. R. Willis, R. Bullough, and S. C. Jain, J. Appl. Phys. **73**, 8297 (1993).
[24]T. J. Gosling, R. Bullough, S. C. Jain, and J. R. Willis, J. Appl. Phys. **73**, 8267 (1993).
[25]A. Atkinson and S. C. Jain, J. Appl. Phys. **72**, 2242 (1992).
[26]A. Atkinson and S. C. Jain, J. Appl. Phys. **76**, 1598 (1994).
[27]J. R. Willis, S. C. Jain, and R. Bullough, Philos. Mag. A **62**, 115 (1990).
[28]L. B. Freund, J. Appl. Phys. **68**, 2073 (1990).
[29]H. M. Zbib and T. D. de la Rubia, Int. J. Plast. **18**, 1133 (2002).
[30]H. M. Zbib, M. Rhee, and J. P. Hirth, *3D Simulation of Curved Dislocations: Discretization and Long Range Interactions* (Pergamon, London, 1996), pp. 15–20.
[31]P. Pant, K. W. Schwarz, and S. P. Baker, Acta Mater. **51**, 3243 (2003).
[32]K. W. Schwarz and J. Tersoff, Appl. Phys. Lett. **69**, 1220 (1996).
[33]K. W. Schwarz, J. Appl. Phys. **85**, 120 (1999).
[34]H. M. Zbib, M. Rhee, and J. P. Hirth, Int. J. Mech. Sci. **40**, 113 (1998).
[35]J. P. Hirth and J. Lothe, *Theory of Dislocations*, 2nd ed. (Krieger, Malabar, FL, 1982).
[36]D. Mitlin, A. Misra, V. Radmilovic, M. Nastasi, R. G. Hoagland, D. J. Embury, J. P. Hirth, and T. E. Mitchell, Philos. Mag. **84**, 719 (2004).
[37]R. Madec, B. Devincre, L. Kubin, T. Hoc, and D. Rodney, Science **301**, 1879 (2003).
[38]F. Akasheh, H. M. Zbib, J. P. Hirth, R. G. Hoagland, and A. Misra (unpublished).

Downloaded 03 Nov 2009 to 128.12.160.33. Redistribution subject to AIP license or copyright; see http://jap.aip.org/jap/copyright.jsp